ChemSystemsChem

Communications
doi.org/10.1002/syst.202100036

Chemistry Europe
European Chemical Societies Publishing

www.chemsystemschem.org

Special Collection

Functional Multivesicular Structures with Controlled Architecture from 3D-Printed Droplet Networks

Alessandro Alcinesio,* Ravinash Krishna Kumar, and Hagan Bayley*[a]

Vesicles are versatile drug delivery systems and a fundamental chassis from which to build synthetic cells. Multivesicular structures, composed of multiple lipid-bound compartments, could form systems with complex functionalities and recapitulate collective behaviour found in living tissues. However, control over number, composition, and arrangement of compartments within multivesicular structures has been limited. Here, we generate multivesicular structures composed of hundreds of lipid-bound compartments arranged in precisely controlled geometries. Through a dewetting process, we transfer 3D-printed droplet networks from oil to aqueous phase and obtain multivesicular structures with designed, complex architectures stable for weeks. We encapsulate membraneless coacervate sub-compartments within the lipid-bound compartments of the 3D-printed multivesicular structures. Further, we use the multivesicular structures as a platform to build synthetic tissues that interact with the external aqueous environment by releasing or sensing molecules and ions. Finally, we build synthetic tissues that synthesize proteins encoded by encapsulated genes.

Synthetic cell-like compartments are of increasing interest for the targeted delivery of drugs,[1] to build smart devices,[2] and to study the emergence of life on our planet.[3,4] Examples of these compartments include water-in-oil droplets,[5,6] vesicles,[7,8] polymersomes,[9] proteinosomes,[10] and coacervate droplets.[11] Sophisticated structures can also be built by encapsulating sub-compartments within these compartments.[12–15] Several cell-like functions have been demonstrated with these systems, such as the compartmentalization of chemical and biochemical reactions,[15–18] division[19,20] and motion.[21] Populations of separate synthetic cells able to communicate with each other have also been developed.[22]

[a] *Dr. A. Alcinesio, R. Krishna Kumar, Prof. H. Bayley*
Department of Chemistry
University of Oxford
12 Mansfield Road, Oxford, OX1 3TA (UK)
E-mail: a.alcinesio@gmail.com
hagan.bayley@chem.ox.ac.uk

Supporting information for this article is available on the WWW under https://doi.org/10.1002/syst.202100036

An invited contribution to a Special Collection on Protocells and Prebiotic Systems.

Synthetic multicompartment structures have also been constructed, with the aim of replicating the more complex functions of living tissues.[23] Among these, networks of droplets in oil interconnected by lipid bilayers have shown great promise for the fabrication of bio-inspired devices.[5,6,24,25] By 3D-printing large droplet networks,[26] precisely patterned synthetic tissues can be built[27,28] and complex collective properties can emerge, such as macroscopic shape change[26] and the transmission of electrical[26,28,29] or chemical[30] signals. However, 3D-printed droplet networks are confined to an oil environment, limiting their applicability under physiological conditions.

Current examples of synthetic multicompartment structures that can function in an aqueous environment are multisomes[31–33] (droplet networks encapsulated within an oil drop immersed in an aqueous solution) and multivesicular liposomes[34–37] (multisome structures where the oil phase is completely removed). These structures can be endowed with functional properties, such as the ability to support cascade reactions,[36] release molecules in a controlled manner[31,33] and perform protein synthesis by transcription and translation.[33,38] However, multisomes and multivesicular liposomes suffer from low production yields and instability.[25] Additionally, multivesicular liposomes composed of only up to 30 non-patterned compartments have been demonstrated so far.[37]

Here, we use 3D-printed droplet networks in oil as a starting template to generate versatile and long-lasting multivesicular structures composed of hundreds of heterogeneous compartments arranged in defined architectures within an aqueous environment. To generate our starting templates, we 3D-printed picolitre-sized aqueous droplets (100 μm diameter, ~520 pL droplet volume) within an oil bath containing the lipid 1,2-diphytanoyl-*sn*-glycero-3-phosphocholine (DPhPC) to form 3D networks of hundreds of droplets interconnected by interface lipid bilayers, as previously described[26,28] (Figure 1a, Supplementary Experimental Section). After printing, we placed large droplets of external aqueous solution around the 3D-printed droplet template. These large external droplets spread on the 3D-printed droplet templates, as well as on the glass surface of the printing container, and then coalesced with each other, forming even larger droplets of external aqueous solution engulfing the 3D-printed droplet templates (Figure 1b). More external aqueous solution was then injected into the large external droplets until the bulk oil phase was completely replaced. Key to the successful dewetting of the structure and the formation of a lipid bilayer at the interface between the 3D-printed aqueous compartments and the external aqueous phase was control of the interfacial tensions within the system[37,39] (see Supplementary Experimental Section). In our

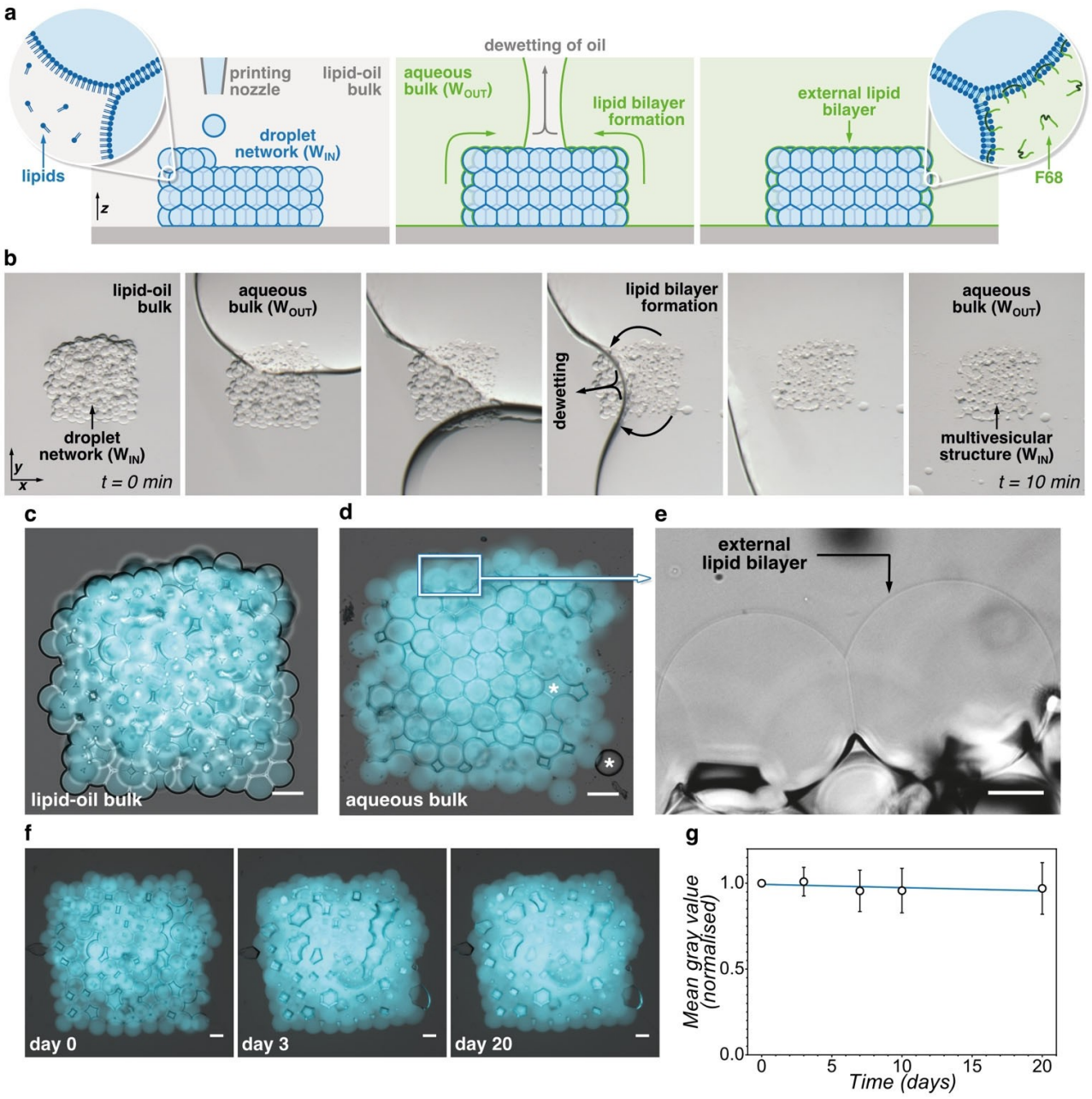

Figure 1. Formation of multivesicular structures by phase transfer of 3D-printed droplet networks into an aqueous environment. (a) The phase transfer process. Networks of picoliter-sized droplets are first 3D-printed within an oil bath containing lipids. Large droplets of an aqueous solution are then added around the printed structure. Removal of the oil phase by a dewetting process and formation of a lipid bilayer at the interface between the network and the external solution is driven by the addition of surfactant block copolymer Pluronic® F68 to the bulk aqueous solution. As depicted, the phase transferred structures remain attached to the printing substrate. (b) Brightfield microscopy images showing the phase transfer of a 3D-printed droplet network. (c, d) Composite brightfield and fluorescence microscopy images of a 3D-printed structure encapsulating a water-soluble dye (Atto488) before (c) and after (d) transfer. Stars indicate examples of residual oil trapped within or at the periphery of the phase transferred structure. (e) Brightfield microscopy image of the area highlighted in (d). (f) Composite brightfield and fluorescence microscopy images of a multivesicular structure containing Atto488 at 0, 3, and 20 days after phase transfer to an aqueous environment. (g) Plot of the mean total fluorescence intensity in multivesicular structures over a 20 day period. The structures shown in (b–f) are composed of 7×8×4 (in x, y and z directions, respectively) compartments. Scale bars: (c, d) 150 μm, (e) 25 μm, (f) 100 μm.

system, the interfacial tensions were controlled in a two-step phase transfer process. Firstly, the lipids in the oil bath were exchanged from DPhPC to 1-palmitoyl-2-oleoyl-*sn*-glycero-3-phosphocholine (POPC); secondly, the triblock copolymer surfactant Pluronic® F68 was included in the external aqueous solution. The use of POPC, which forms lipid bilayers of lower interfacial tension compared to DPhPC,[28] promoted fast and efficient dewetting of the oil phase from the 3D-printed templates by maintaining the concentration of F68 at a minimum (see Supplementary Experimental Section). By using

this method, we could generate 3D multivesicular structures consisting of hundreds of lipid-bound compartments from 3D-printed droplet networks, without disruption of the architecture of the starting droplet template or loss of encapsulated cargo (Figure 1c–e and S1). Additionally, we monitored the stability of the generated multivesicular structures and observed no significant rearrangement of the compartments, and importantly no loss of encapsulated fluorescent cargo for weeks, demonstrating the presence of impermeable lipid bilayers around the transferred structure (Figure 1f, g).

Next, we generated 3D multivesicular structures composed of hundreds of heterogeneous compartments patterned in precise architectures (Figure 2). We used patterned 3D-printed droplet networks in oil as starting templates, obtained by synchronized printing of multiple aqueous solutions into designed architectures.[26,28] We 3D-printed two types of droplet templates, one composed of two populations of compartments arranged in a core-shell architecture (224 compartments in total, Figure 2a), and one composed of 4 populations of compartments, in which one population formed a Y-shaped

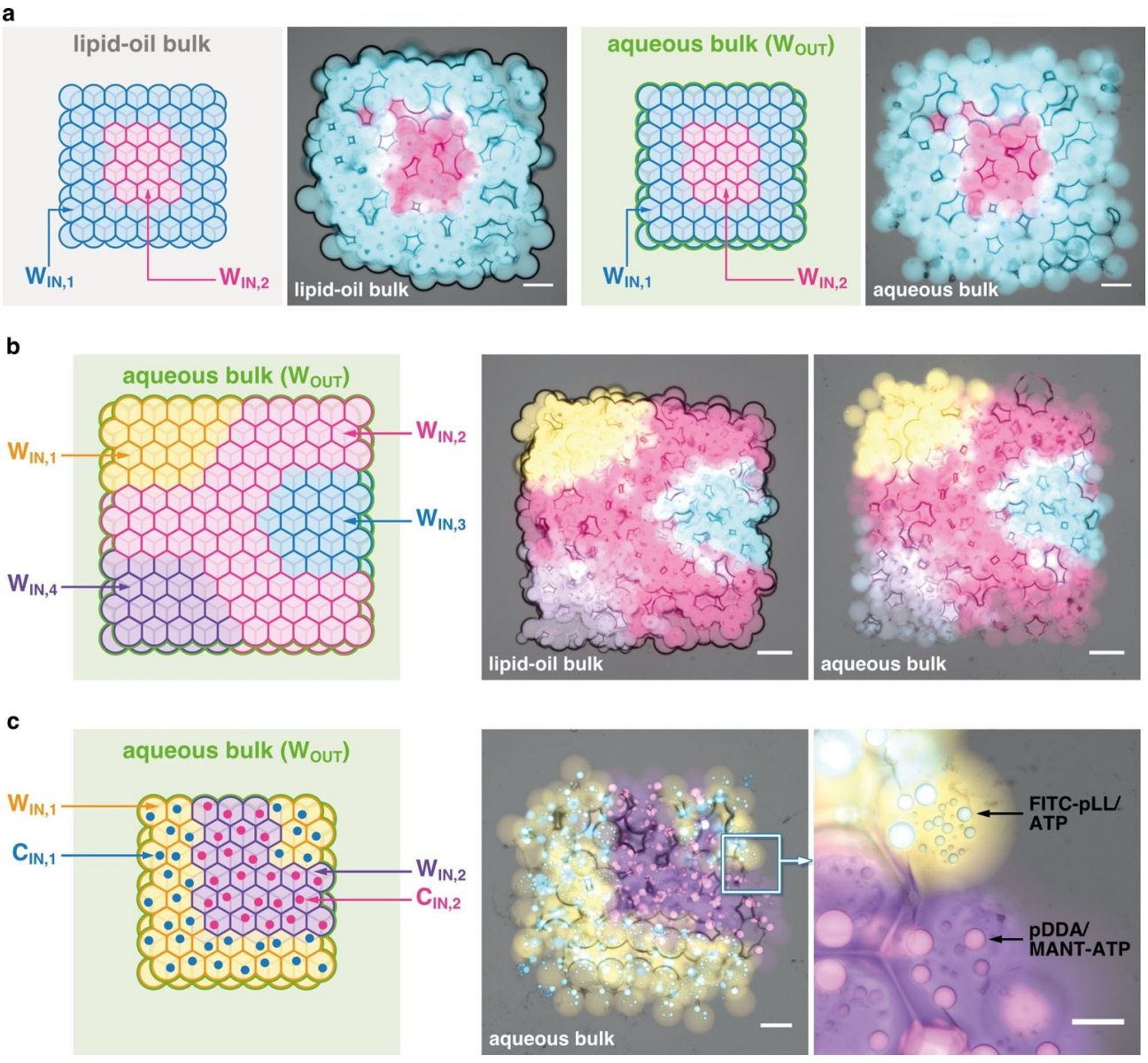

Figure 2. Complex architectures in multivesicular structures. (a) Diagrams and composite brightfield and fluorescence microscopy images of a multivesicular structure with 2 populations of compartments, $W_{IN,1}$ (cyan) and $W_{IN,2}$ (magenta), patterned in a core-shell architecture, before (left) and after (right) phase transfer to an aqueous environment, W_{OUT}. (b) Diagrams and composite brightfield and fluorescence microscopy images of a multivesicular structure composed of 4 encapsulated aqueous phases, $W_{IN,1}$ (yellow), $W_{IN,2}$ (magenta), $W_{IN,3}$ (cyan) and $W_{IN,4}$ (lilac), patterned in a Y-shaped architecture. (c) Diagram and composite brightfield and fluorescence microscopy images of a multivesicular structure with an L-shaped pattern, encapsulating distinct coacervate sub-compartments within each compartment type. $W_{IN,1}$ (yellow) compartments contain $C_{IN,1}$ (cyan) coacervate sub-compartments composed of pLL/ATP, while $W_{IN,2}$ (lilac) compartments contain $C_{IN,2}$ (magenta) coacervate sub-compartments composed of pDDA/ATP. The structures shown in (a, c) are composed of $7\times8\times4$ (in x, y and z directions, respectively) compartments in total, while the structure in (b) is composed by $10\times11\times5$ (in x, y and z directions, respectively) compartments in total. Scale bars, (a) 150 μm, (b) 200 μm, (c) 150 μm (left) and 25 μm (right).

path and was surrounded by the remaining 3 populations (550 compartments in total, Figure 2b). After phase transfer, the resulting multivesicular structures maintained their structural integrity and the compartment architectures imposed by the 3D-printed droplet templates (Figure 2a, b).

In living tissues, populations of specialized cells carry out specific functions within the tissues.[40,41] Inside these cells, subcellular compartments carry out distinct tasks, such as transcriptional regulation, energy generation and waste disposal.[41,42] To investigate the ability of our system to mimic the hierarchical organization found in cells and tissues, we incorporated coacervate droplets within the patterned compartments. We patterned 2 populations of compartments to form an L-shaped architecture, with each population containing coacervate sub-compartments of different compositions, one consisting of poly-L-lysine (pLL) and adenosine triphosphate (ATP), the other of poly(diallyldimethylammonium) (pDDA) and ATP. We successfully encapsulated the coacervate sub-compartments within the respective populations of lipid-bound compartments, preserving their distinct chemical compositions, and generated structures with hierarchical organization (Figure 2c).

After forming multivesicular structures with complex architectures, we then sought to use these structures as chassis to build synthetic tissues able to interact with the external aqueous environment (Figure 3). We functionalized the lipid bilayers between the compartments and between the structures and the external environment with the pore-forming membrane protein α-hemolysin (αHL), thereby allowing the selective diffusion of small molecules throughout the synthetic tissue and to or from the external solution (Figure 3a, d).[43] We first encapsulated 2-[*N*-(7-nitrobenz-2-oxa-1,3-diazol-4-yl) amino]-2-deoxy-D-glucose (2-NBDG) within the synthetic tissue's compartments and monitored its release over time. We monitored the release of 2-NBDG using a laser scanning confocal microscope (Leica SP5) focused at the midpoint of the first compartment layer (at the bottom) of the synthetic tissue, to exclude the contribution of the upper layers from our analysis. In the presence of αHL, 2-NBDG was released from the

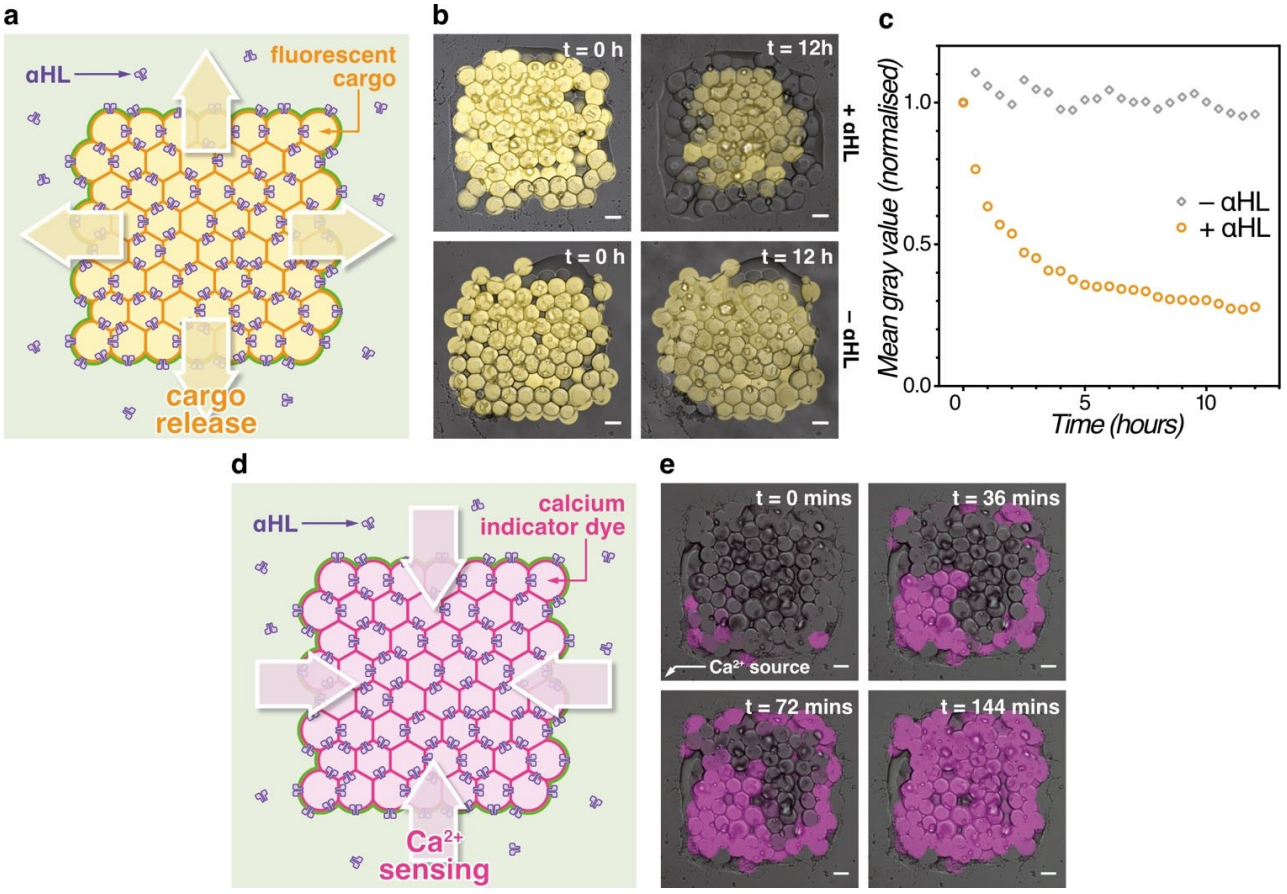

Figure 3. Chemical communication with the external aqueous environment. (a) A synthetic tissue releasing molecular cargo into the external solution. The lipid bilayers that separate the synthetic compartments from each other and from the external solution are permeabilized by αHL. (b) Composite brightfield and fluorescence microscopy images showing the release over time of a fluorescent cargo (2-NBDG) from a synthetic tissue functionalized with αHL (top). No release is observed in the absence of αHL (bottom). (c) Mean total fluorescence intensity versus time for the experiments in (b). The data is normalized over the initial value at time = 0 h. (d) A synthetic tissue reporting Ca^{2+} ions in the external solution. All lipid bilayers in the structure are permeabilized by αHL. A membrane-impermeant calcium indicator fluorescent dye (Rhod-dextran) is encapsulated within each compartment. (e) Composite brightfield and fluorescence microscopy images showing the increase in fluorescence of the compartments over time after addition of Ca^{2+} ions to the external solution. The arrow indicates the location where the $CaCl_2$ solution was added. The structures shown in (b, e) are composed of 7×8×4 (in x, y and z directions, respectively) compartments. Scale bars, 100 μm.

synthetic tissue, while no significant change in fluorescence was detected without αHL after 12 h (Figure 3b, c). These observations confirmed that functional αHL channels were formed both in the internal lipid bilayers (interconnecting the compartments with each other) and the bilayers interfacing the synthetic tissue with the external aqueous environment. Furthermore, the release of fluorescent cargo started from the compartments located at the periphery and depletion proceeded inwards (Figure 3b). This phenomenon suggests that the diffusion of 2-NBDG through the membrane pores is the rate limiting step in the passive diffusion of solutes from the core of the synthetic tissue to the external environment.

Another fundamental function found in biological tissues is the ability to detect and respond to chemical cues in the environment. To mimic this behaviour, we generated a synthetic tissue in which all lipid bilayers in the structure were functionalized with αHL. Additionally, we encapsulated a membrane-impermeant calcium indicator dye (Rhod-dextran, MW 10000) within the compartments (Figure 3d). We monitored the diffusion of Ca^{2+} and its binding to the indicator dye by confocal microscopy, focusing on the first compartment layer (at the bottom) of the synthetic tissue. Upon $CaCl_2$ addition to the external aqueous solution, we observed an increase in fluorescence over time within the synthetic tissue, starting from the compartments located at the periphery of the structure (Figure 3d). Within 2.5 h, we observed homogeneous fluorescence in all compartments of the synthetic tissue, indicating that calcium had diffused throughout the structure. Interestingly, compartments closer to the source of the Ca^{2+} signal showed a faster increase in fluorescence compared to other regions of the synthetic tissue (Figure 3e). This observation indicates that synthetic tissues have the ability to detect gradients of chemical cues in the external environment.

Lastly, to demonstrate the compatibility of our structures with complex biological processes found in living cells, we carried out protein synthesis by transcription and translation within our synthetic tissues (Figure 4a). We 3D-printed the template structure encapsulating the "protein synthesis using recombinant elements" (PURE) system, which contains a minimal set of components required for cell-free protein synthesis.[44,45] Along with the PURE system, we also encapsulated a plasmid encoding the Emerald green fluorescent protein under control of a T7 promoter. We then successfully transferred the 3D-printed template to an aqueous environment. The resulting synthetic tissue was stable for at least 18 h and expressed the fluorescent protein. No protein expression was detected if the plasmid DNA was omitted (Figure 4b).

In summary, we report a versatile strategy to generate multivesicular structures composed of hundreds of compartments arranged in precisely controlled architectures. The resulting structures preserve their architecture and are stable for weeks. Using our strategy, we have encapsulated membraneless sub-compartments as organelle mimics within specific populations of compartments, demonstrating hierarchical organization within synthetic tissues. We have also generated synthetic tissues that interact with the surrounding aqueous environment by releasing or sensing molecules and ions. Lastly, we built synthetic tissues that express proteins by transcription and translation. We believe our approach is a steppingstone towards advanced synthetic multicellular systems that can communicate with living cells and tissues with precise spatial and temporal control.

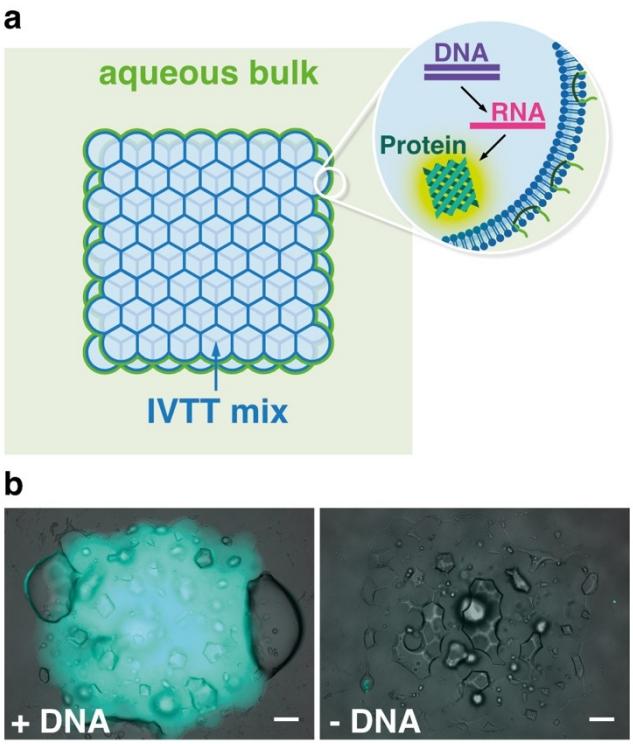

Figure 4. Synthesis of proteins within synthetic tissues. (a) A synthetic tissue in an aqueous environment encapsulating the machinery for protein synthesis by transcription and translation (IVTT, PURExpress). (b) Composite brightfield and fluorescence microscopy images of synthetic tissues with encapsulated IVTT machinery, with (left) or without (right) DNA encoding for the Emerald green fluorescent protein. The structure shown in (b) is composed of 7×8×4 (in x, y and z directions, respectively) compartments. Scale bars, 100 μm.

Acknowledgements

This work was supported by a European Research Council Advanced Grant. AA acknowledges funding from the University of Oxford, the EPSRC & BBSRC Centre for Doctoral Training in Synthetic Biology (grant EP/L016494/1), the Cyril & Phillis Long Studentship, and the Clarendon Fund Scholarship. The authors thank Idil Cazimoglu for generating αHL protein and plasmid in this work. The authors also thank Michael J. Booth for insightful discussions on protein synthesis by transcription and translation.

Conflict of Interest

The authors declare no conflict of interest.

Keywords: 3D-printing · coacervates · liposomes · synthetic cells · synthetic tissues

[1] F. Lussier, O. Staufer, I. Platzman, J. P. Spatz, *Trends Biotechnol.* **2020**, *39*, 445–459, https://doi.org/10.1016/j.tibtech.2020.08.002.
[2] B. C. Buddingh', J. C. M. van Hest, *Acc. Chem. Res.* **2017**, *50*, 769–777, https://pubs.acs.org/doi/10.1021/acs.accounts.6b00512.
[3] P. Walde, R. Wick, M. Fresta, A. Mangone, P. L. Luisi, *J. Am. Chem. Soc.* **1994**, *116*, 11649–11654.
[4] S. S. Mansy, J. P. Schrum, M. Krishnamurthy, S. Tobé, D. A. Treco, J. W. Szostak, *Nature* **2008**, *454*, 122–125.
[5] M. A. Holden, D. Needham, H. Bayley, *J. Am. Chem. Soc.* **2007**, *129*, 8650–8655.
[6] H. Bayley, B. Cronin, A. Heron, M. A. Holden, W. L. Hwang, R. Syeda, J. Thompson, M. Wallace, *Mol. BioSyst.* **2008**, *4*, 1191–1208.
[7] J. C. Blain, J. W. Szostak, *Annu. Rev. Biochem.* **2014**, *83*, 615–640.
[8] S. Deshpande, Y. Caspi, A. E. C. Meijering, C. Dekker, *Nat. Commun.* **2016**, *7*, 10447, https://www.nature.com/articles/ncomms10447.
[9] K. T. Kim, J. J. L. M. Cornelissen, R. J. M. Nolte, J. C. M. van Hest, *Adv. Mater.* **2009**, *21*, 2787–2791.
[10] X. Huang, M. Li, D. C. Green, D. S. Williams, A. J. Patil, S. Mann, *Nat. Commun.* **2013**, *4*, 1–9, https://www.nature.com/articles/ncomms3239.
[11] A. F. Mason, B. C. Buddingh', D. S. Williams, J. C. M. van Hest, *J. Am. Chem. Soc.* **2017**, *139*, 17309–17312.
[12] R. J. R. W. Peters, M. Marguet, S. Marais, M. W. Fraaije, J. C. M. van Hest, S. Lecommandoux, *Angew. Chem. Int. Ed.* **2014**, *53*, 146–50; *Angew. Chem.* **2014**, *126*, 150–154.
[13] W. T. S. Huck, N. Deng, *Angew. Chem. Int. Ed.* **2017**, *56*, 9736–9740; *Angew. Chem.* **2017**, *129*, 9868–9872, https://onlinelibrary.wiley.com/doi/10.1002/anie.201703145.
[14] S. Deshpande, F. Brandenburg, A. Lau, M. G. F. Last, W. K. Spoelstra, L. Reese, S. Wunnava, M. Dogterom, C. Dekker, *Nat. Commun.* **2019**, *10*, 1800, https://www.nature.com/articles/s41467-019-09855-x.
[15] C. Love, J. Steinkühler, D. T. Gonzales, N. Yandrapalli, T. Robinson, R. Dimova, T.-Y. D. Tang, *Angew. Chem. Int. Ed.* **2020**, *59*, 5950–5957; *Angew. Chem.* **2020**, *132*, 6006–6013.
[16] T. Oberholzer, K. H. Nierhaus, P. L. Luisi, *Biochem. Biophys. Res. Commun.* **1999**, *261*, 238–241.
[17] S. Thutupalli, S. Herminghaus, *Eur. Phys. J. E* **2013**, *36*, 91, https://link.springer.com/article/10.1140/epje/i2013-13091-2.
[18] G. Jones, P. H. King, H. Morgan, M. R. R. de Planque, K. P. Zauner, *Artif. Life* **2015**, *21*, 195–204.
[19] T. F. Zhu, J. W. Szostak, *J. Am. Chem. Soc.* **2009**, *131*, 5705–5713.
[20] J. Steinkühler, R. L. Knorr, Z. Zhao, T. Bhatia, S. M. Bartelt, S. Wegner, R. Dimova, R. Lipowsky, *Nat. Commun.* **2020**, *11*, 905, https://www.nature.com/articles/s41467-020-14696-0.
[21] L. K. E. A. Abdelmohsen, M. Nijemeisland, G. M. Pawar, G. J. A. Janssen, R. J. M. Nolte, J. C. M. van Hest, D. A. Wilson, *ACS Nano* **2016**, *10*, 2652–2660.
[22] B. C. Buddingh', J. Elzinga, J. C. M. van Hest, *Nat. Commun.* **2020**, *11*, 1652, https://www.nature.com/articles/s41467-020-15482-8.
[23] D. T. Gonzales, C. Zechner, T. Y. D. Tang, *Curr. Opin. Syst. Biol.* **2020**, *24*, 56–63.
[24] G. Maglia, A. J. Heron, W. L. Hwang, M. A. Holden, E. Mikhailova, Q. Li, S. Cheley, H. Bayley, *Nat. Nanotechnol.* **2009**, *4*, 437–440.
[25] M. J. Booth, V. Restrepo Schild, F. G. Downs, H. Bayley, *Mol. BioSyst.* **2017**, *13*, 1658–1691.
[26] G. Villar, A. D. Graham, H. Bayley, *Science* **2013**, *340*, 48–52.
[27] M. J. Booth, V. Restrepo Schild, S. J. Box, H. Bayley, *Sci. Rep.* **2017**, *7*, 9315, https://www.nature.com/articles/s41598-017-09394-9.
[28] A. Alcinesio, O. J. Meacock, R. G. Allan, C. Monico, V. Restrepo Schild, I. Cazimoglu, M. T. Cornall, R. Krishna Kumar, H. Bayley, *Nat. Commun.* **2020**, *11*, 2105, https://www.nature.com/articles/s41467-020-15953-y.
[29] M. J. Booth, V. R. Schild, A. D. Graham, S. N. Olof, H. Bayley, *Sci. Adv.* **2016**, *2*, 1–12, https://www.science.org/doi/10.1126/sciadv.1600056.
[30] A. Dupin, F. C. Simmel, *Nat. Chem.* **2019**, *11*, 32–39.
[31] G. Villar, A. J. Heron, H. Bayley, *Nat. Nanotechnol.* **2011**, *6*, 803–808.
[32] Y. Elani, X. C. I. Solvas, J. B. Edel, R. V. Law, O. Ces, *Chem. Commun.* **2016**, *52*, 5961–5964.
[33] M. J. Booth, I. Cazimoglu, H. Bayley, *Commun. Chem.* **2019**, *2*, 1–8, https://www.nature.com/articles/s42004-019-0244-y.
[34] S. Mantripragada, *Prog. Lipid Res.* **2002**, *41*, 392–406.
[35] Y. Elani, A. Gee, R. V. Law, O. Ces, *Chem. Sci.* **2013**, *4*, 3332.
[36] Y. Elani, R. V. Law, O. Ces, *Nat. Commun.* **2014**, *5*, 5305, https://www.nature.com/articles/ncomms6305.
[37] N.-N. Deng, M. Yelleswarapu, W. T. S. Huck, *J. Am. Chem. Soc.* **2016**, *138*, 7584–7591.
[38] Y. Elani, R. V. Law, O. Ces, *Phys. Chem. Chem. Phys.* **2015**, *17*, 15534–15537.
[39] S. Torza, S. G. Mason, *Science* **1969**, *163*, 813–814.
[40] G. Bell, A. O. Mooers, *Biol. J. Linn. Soc.* **1997**, *60*, 345–363.
[41] T. Gabaldón, A. A. Pittis, *Biochimie* **2015**, *119*, 262–268.
[42] S. F. Banani, H. O. Lee, A. A. Hyman, M. K. Rosen, *Nat. Rev. Mol. Cell Biol.* **2017**, *18*, 285–298.
[43] I. Cazimoglu, M. J. Booth, H. Bayley, **2021**, bioRxiv preprint DOI: 10.1101/2021.05.05.442835, https://www.biorxiv.org/content/10.1101/2021.05.05.442835v1.
[44] Y. Shimizu, A. Inoue, Y. Tomari, T. Suzuki, T. Yokogawa, K. Nishikawa, T. Ueda, *Nat. Biotechnol.* **2001**, *19*, 751–755.
[45] Y. Shimizu, T. Kanamori, T. Ueda, *Methods* **2005**, *36*, 299–304.

Manuscript received: July 28, 2021
Accepted manuscript online: August 23, 2021
Version of record online: September 14, 2021